Article

Insights into the Engineered Gold Nanoparticle-Based Remedy for Supplementation Therapy of Ovarian Carcinoma

Muhammad Umar Farooq,* Alexey P. Dovzhenko, Rustem R. Zairov, Gulmira Abyzbekova, Moussab Harb, Bassim Arkook, Nurgali Akylbekov, Anipa Tapalova,* and Mohamed M. Makhlouf*

Read Online

ACCESS | Metrics & More | Article Recommendations

ABSTRACT: Chronic diseases, notably cancer, pose a significant global threat to human life. Oncologists and medical professionals addressing malignancies confront challenges such as toxicity and multidrug resistance. To tackle these issues, the focus has shifted toward the employment of multifunctional colloidal gold nanoparticles. This study aims to design pH-sensitive doxorubicin-loaded gold nanoparticles using polyvinylpyrrolidone. The cytotoxic efficacy of the designed gold nanoarchitecture and its doxorubicin counterpart was assessed in an in vitro model using the HeLa cell. In comparison to the free drug, experimental evaluations showed that the gold nanoarchitecture outperformed significantly lower unspecific drug leaching and efficiently delivered the payload in a controlled manner, boosting the chemotherapy outcomes. This work opens a streamlined approach for engineering gold nanoarchitecture that could be further expanded to incorporate other therapeutics and/or functional moieties that require optimized controlled delivery, offering a one-size-fits-all solution and paving the revolutionary adjustments to healthcare procedures.
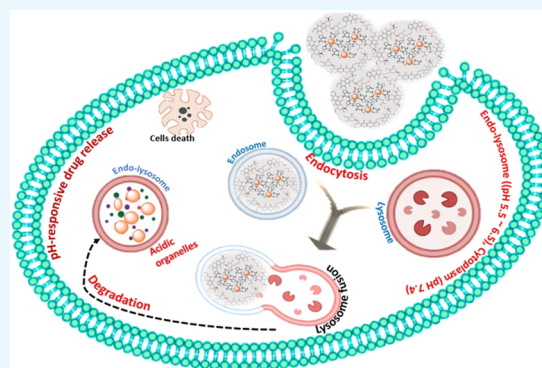
1. INTRODUCTION

According to most definitions, cancer is characterized as a complex chronic disease, hallmarked by abnormal cell growth, tissue invasion, and metastasis beyond its usual boundaries, threatening public health worldwide.[1] Normally, behavioral and dietary risks, lack of physical activity, high body mass index, smoking, alcohol consumption, and contact with toxic chemicals or radiation are the external factors involved in DNA mutations and cancer growth.[2] Cancers, including approximately 70% of new cases every year, are anticipated to witness a distressing surge in mortality rates. According to the World Health Organization (WHO), characterized by its complexity and heterogeneity, cancer is still among the leading causes of fatalities, accounting for an estimated one in six mortalities.[1] The cancer-related mortality rate in low- and middle-income countries is very high compared to that of other diseases. Late-stage diagnosis, lack of safety clinical assessments, and expensive pathological services are the common hindrances in the war against cancer. In addition, conventional cancer treatment options are limited to surgery, chemotherapy, and radiotherapy. The key concerns that link each of these treatment methods are their multiple side effects, risk of damage to healthy tissues, and possibility of falling short of completely eradicating cancer.[3] Giving more intensive chemotherapy or radiotherapy dosages improves short-term out-comes but also increases the risk of mortality and morbidity as a consequence of treatment failures and substantial incidence in healthcare costs. Physicians and healthcare systems need to focus on the growing cognizance that cancer patients can and should play an essential role in defining the rationalizing of optimal care, with counter-arguments to demonstrate what is safe and what is affordable, as not all patients need or respond to identical treatments.[4]
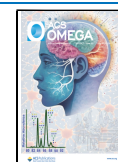
Nanomedicine, an offshoot of nanotechnology, is an exponentially emerging and rapidly evolving field, and the use of nanoparticles (NPs), particularly gold nanoarchitecture (GNPs),[5] is attractive to candidates due to their unique physicochemical properties. They are extensively used in research for their applications in biomedicine with relatively high biocompatibility, synergistic therapeutic efficacy, and capability for less off-target toxicity.[6] During the last three decades, clinical assessment improvements have changed cancer management dramatically. However, nanoparticle-

based less toxic and effective therapeutic strategies have provided inspirational tools to combat the leading concerns of cancers that are otherwise difficult to treat, introducing their capability to evade existing mechanisms of drug resistance.[7] Recently, research on a variety of NP-based therapies has increased rapidly with the promise of efficient site-specific drug delivery against a range of chronic diseases for better treatment outcomes.[8] Although small compared to cells, NPs are large enough to give them the capability to encapsulate novel therapeutic agents, which can be of multiple types used for chronic ailment treatment.[9] In addition, NPs functionalized with therapeutic drugs or macromolecules such as peptides, ligands, nucleic acids, genes, aptamers, or antibodies have shown potential to be used as nanomedicines after passing clinical trials.[8] As a piece of evidence, all of this can add up to a decreased risk to the patient and is capable of improving the probability of survival.

Indeed, GNPs have been characterized to be excellent for the modulation of cellular uptake and cell penetration without disrupting the phospholipid bilayer.[10] Conversely, the clinical translation rate of GNPs has not followed the prognostic market studies, which are mainly associated with the chemistry of GNP-based nanomedicines.[11] For the clinical management of cancers, Astra Zeneca, in partnership with Cytimmune, has developed a novel Aurimune (CYT-6091) GNP-based nanomedicine for human use.[12] Many other GNP-based remedies, such as Auroshell, Aurimune, and CYT-21625, are striving for clinical approval.[12] These nanostructured gold architecture systems may be one of the most recommended cancer treatment options in the future that must overcome limitations such as adverse reactions, low specificity of chemotherapeutic drugs, and multidrug resistance associated with conventional cancer treatment strategies.[13] Nevertheless, extensive clinical trials are still required to ensure the long-term benefits and risks of treatments, along with new methodologies to detect, diagnose, and reduce the risk of disease for nanomedicines in humans.

In oncology, GNPs emerged as a potential candidate for detection, pharmaceutical delivery systems, and targeting of specific cells or tissues.[14−16] Moreover, GNPs possess a unique localized surface plasmon resonance (LSPR), an optical phenomenon generated by a specific wavelength of light when it interacts with electrons on the surface of nanostructured gold architecture.[17] The LSPR can also be tuned by altering different aspect ratios, morphology, shape, and interparticle spacing. When small spherical GNPs are irradiated with light, this subsequently causes a collective coherent oscillation of conduction band electrons.[17,18] Surface engineering of GNPs and their resistance to corrosion and oxidation make them particularly attractive for nanomedicine applications. In addition, GNPs have been effectively used in various domains, including cancer diagnosis probes,[7,11,18] drug delivery, and contrast agents,[14,19] and are suitable for the multifaceted photothermic treatment of cancer.[18,20] Moreover, the nanostructured gold architecture-based drug delivery platforms are attractive owing to the universal pathophysiological phenomenon that refers to the enhanced permeability and retention (EPR) effect, while NP-based delivery has been interrogated by a meta-analysis which estimated that the median delivery efficiency is only 0.7%.[21] The authors argue that this relatively low delivery efficiency is a hurdle for nanomedicine clinical translation, particularly in the case of doxorubicin.[21]

Doxorubicin (DOX) has Food and Drug Administration (FDA) approval to be used as an anthracycline antitumor drug, often prescribed in combination with other medications to treat certain types of acute leukemias, lymphomas, and cancers of the ovary, uterus, breast, and lung.[14,16] DOX is a commercially available anthracycline antitumor drug generally administered by injection or via an intravenous infusion. Regrettably, when administered directly, the therapeutic potential of DOX is limited by extensive adverse event profiles ranging from mild to severe including infection, skin hyperpigmentation, vomiting, peripheral neuropathy, especially life-threatening pericarditis—myocarditis or arrhythmias, cardiomyopathy, cardiotoxicity, keratitis, and myelosuppression.[22,23] On the other hand, acute side effects associated with high-dose DOX are more serious and include the growth of multidrug resistance protein (MDR) and the stimulation of permeability glycoprotein (P-gp), an uninhibited drug efflux pump, also known as a major factor of the MDR phenotype in cancer cells, which has been extensively studied due to overexpression and chemotherapy failure in cancer cells.[24]

Researchers are studying alternative strategies, for example, the tuning of anthracyclines and the design of novel drug delivery agents including nanoparticle-assisted delivery systems in the hope of circumventing P-gp-dependent efflux.[9,16,25] General strategies to synthesize DOX-loaded GNPs involve multistep surface functionalization with various biodegradable polymers or functional groups as reducing and functionalizing agents.[16,22] In some cases, under acidic conditions, the protonated DOX was directly conjugated with negatively charged GNPs,[22,26] and DOX molecule encapsulation was done in the presence of oxygen.[25] Polyvinylpyrrolidone or polyvidone (PVP) is a commercially available nonionic water-soluble polymer that binds the drugs strongly to the GNP surfaces.[27] The PVP not only provides greater stability of drug-loaded GNPs and inhibits particle aggregation better than citrate or tannic acid capping agents but also enhances the drug solubility in water or organic solvents.[28] However, most of these synthetic processes involve a series of complicated reactions and harsh chemical intermediates that directly affect the internal organs of patients. Herein, we report a versatile, cost-effective, and simple method to synthesize PVP-GNPs, and their surfaces were tuned with DOX, focusing on the therapeutic options to overcome the MDR obstacles. DOX was loaded onto the PVP-GNPs by direct ionic polymer complexation.[29]

The developed nanostructured architecture (PVP-GNPs-DOX) was investigated for chemotherapeutic delivery and therapeutic effectiveness against the in vitro model of a HeLa cell, a particularly aggressive strain of cervical cancer cells. The PVP-GNPs-DOX was more toxic to HeLa cells than PVP-GNPs or free DOX. Finally, a significant correlation of the in vitro cytotoxicity and tumor inhibition was generated that demonstrates the potential use of PVP-GNPs-DOX nanostructured architecture as a drug carrier platform, suitable for precise targeting, that may present a significant approach to inhibiting the risks of MDR in cancer cells, thus improving chemotherapeutic drug outcomes.

2. RESULTS AND DISCUSSION

The GNPs stabilized using PVP by the dynamic stirring process have received substantial attention in chronic disease diagnosis and cancer therapy. Herein, PVP-GNPs were synthesized and conjugated with DOX for potential biomedical
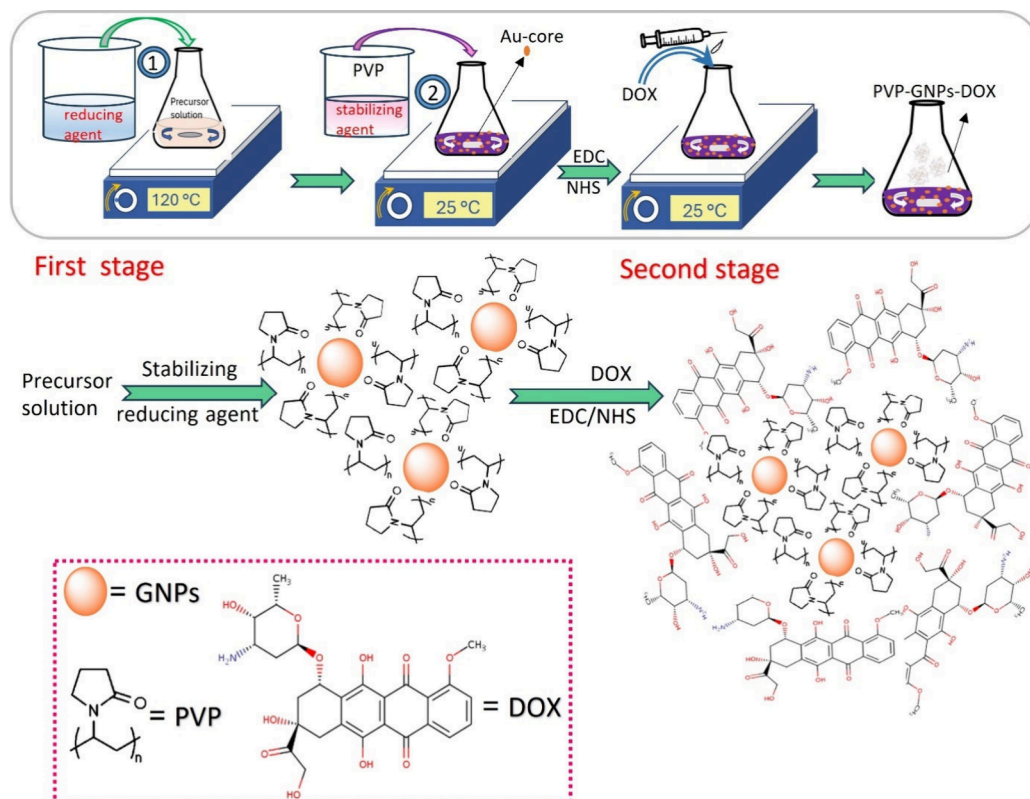
Figure 1. Scheme of the synthesis route of PVP-GNPs and PVP-GNPs-DOX nanoconjugates. The DOX was conjugated on the PVP-GNPs surface via a standard EDC/NHS coupling reaction.

applications. The two-stage synthesis mechanism of PVP-GNPs and PVP-GNPs-DOX nanoconjugates is shown in Figure 1. In the first step, the desired amount of chloroauric acid was reduced by sodium citrate and then stabilized with PVP. In the second step, the PVP-GNPs were used with DOX molecules to design a synergic anticancer therapeutics model. The morphology and electronic properties of as-synthesized PVP-GNPs and PVP-GNPs-DOX were fully characterized using XRD, UV−vis, FTIR, and TEM/HR-TEM techniques.

2.1. XRD Analysis. Figure 2 presents the XRD analysis and crystalline nature of synthesized PVP-GNPs and PVP-GNPs-DOX. As seen for the PVP-GNPs in Figure 2, the XRD pattern exhibited four strong diffraction signals and one weak diffraction signal located at around $2\theta = 38.50$, 44.40, 64.60, 77.55, and 81.80°, matched well to the (111), (200), (220), (311), and (222) planes respectively, indicating the face-centered cubic structure of GNPs. Interestingly, the observed diffraction signals were matched with standard diffraction peaks according to JCPDS number 04-0784,[30] with a predominant intense peak at 38.40° representing the growth in the (111) direction, confirming the crystalline nature of spherical GNPs.[10] In addition, the XRD patterns of PVP-GNPs-DOX (green) showed similar strong diffraction signals at $2\theta = 38.30$, 44.60, 64.70, 77.60, and 81.80° that were indexed to (111), (200), (220), (311), and (222) planes (Figure 2). Other as yet unassigned small peaks were also observed, confirming the PVP presence on the surface of GNPs, thus suggesting the conjugation of PVP and DOX onto GNP surfaces, as intended. Moreover, the peak intensities of gold in PVP-GNPs were similar to that from the PVP-GNPs-DOX, demonstrating that both samples have similar structural features.
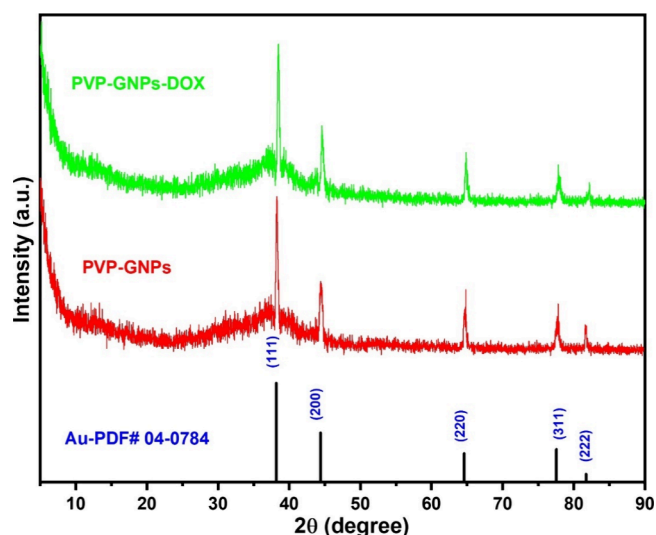

Figure 2. XRD pattern of as-synthesized PVP-GNPs and PVP-GNPs-DOX and comparison with standard JCPDS card no. 04-0784.

2.2. DLS Measurement. The analysis of hydrodynamic particle size and measurement of the surface charge (zeta potential) on particles suspended in a dispersion medium are effective predictors of the stability of colloidal dispersions.[31] Figure 3 shows the dynamic light scattering (DLS) and zeta potential results of PVP-GNPs and PVP-GNPs-DOX. According to DLS measurements, the PVP-GNP sample shows a narrow particle size distribution with an average size of 13.35 ± 2.10 nm (Figure 3A). Upon interaction with DOX molecules, the hydrodynamic size distributions of PVP-GNPs
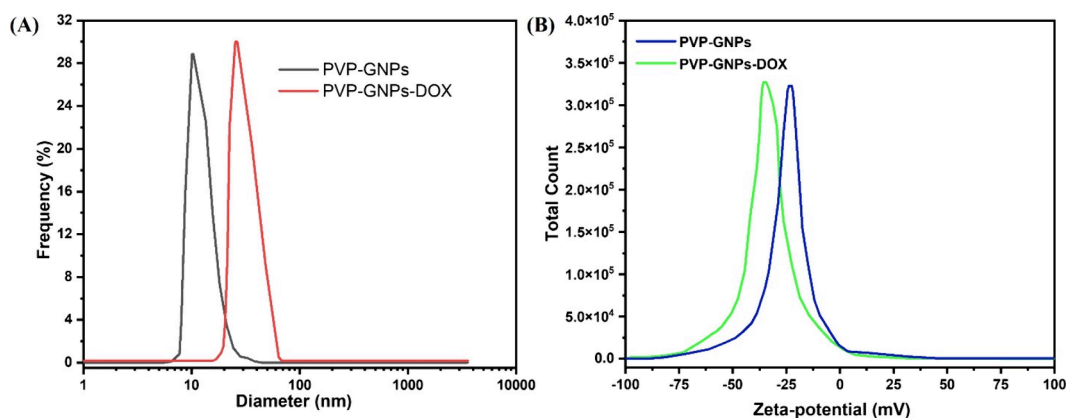
Figure 3. DLS size distribution (A) and zeta potential (B) measurement of as-synthesized PVP-GNPs and PVP-GNPs-DOX.
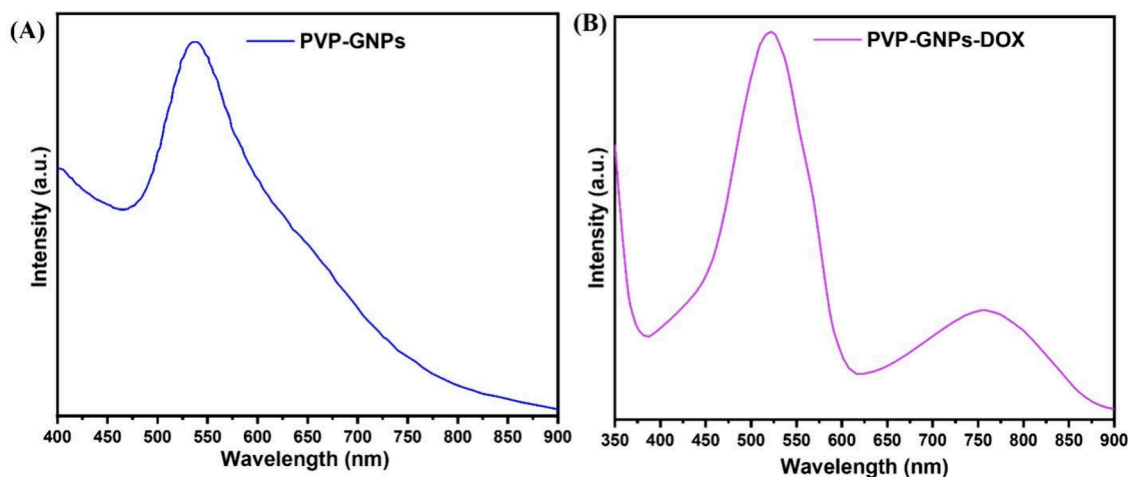

Figure 4. UV−vis spectroscopic changes in the spectra of the as-synthesized PVP-GNPs (A) and PVP-GNPs-DOX (B).

changed from ∼14 to ∼38 nm. Apparently, the particle size distribution had a deep impact on the performance of nanocarrier drug delivery systems. Nanoformulation with a lower zeta potential and a size smaller than 200 nm can offer well-organized inactive tumor-targeting capabilities.[21] Furthermore, the surface modification of PVP-GNPs with DOX was also confirmed by assessing surface charge using zeta-potential measurements. In our case, the surface charges on PVP-GNPs and PVP-GNPs-DOX were around −24.2 and −36.5 mV, respectively (Figure 3B). When the PVP-GNPs are conjugated to DOX, their surface charge was approximately changed from −24.2 and −36.5 mV, proving the interaction between head carbonyl (C=O) groups of PVP and DOX molecules. In addition, the localized surface charge density was shared by the transmission of n electrons from a nucleophilic PVP to DOX molecules. The negatively charged surface of PVP-GNPs and PVP-GNPs-DOX inhibits flocculation, thus stabilizing the colloids by electrostatic repulsion and steric action. The negative zeta potential values confirm the existence of strong electrostatic repulsion between molecules.[31] The dispersed system will be more stable if it has a higher negative charge, which ultimately results in a strong electrostatic repulsive force between the molecules. The functional groups on PVP-GNPs react with the surrounding media when combined with DOX, resulting in creating a surface charge that attracts the accumulation of dissimilar charged ions. Spontaneously, these counterions self-organize into an electrochemical layer.

2.3. UV−Vis Spectroscopy. The ultraviolet−visible (UV−vis) spectral study was performed to analyze the electronic characteristics of PVP-GNPs and PVP-GNPs-DOX. The UV−vis absorption spectra of PVP-GNPs and PVP-GNPs-DOX are presented in Figure 4. A strong absorption maximum band in the range of 517−533 nm was observed for PVP-GNPs, as shown in Figure 4A, which is similar to the SPR characteristic of almost spherical GNPs.[32,33] The morphology, shape, and size of GNPs contribute to spectral characteristics because of the variations in surface polarization. The size and shape of GNPs greatly influence the magnitude of the cross-section absorption and scatter. For example, nonspherical GNPs exhibited multiple red-shifted peaks compared to spherical GNPs. Thus, spherical GNPs in the size range of 10 to 20 nm indicate that absorption is the predominant process.[34] Therefore, the absorption intensity and peak position of SPR signals strongly depend on the morphology, size, and shape of GNPs.[35]

It was observed that the red wine color of the GNP solution absorbs visible light at around 520 nm, which steadily increases the oscillation energy of the surface electrons of the GNPs. Therefore, a sharp SPR occurred at ∼520 nm, confirming the synthesis of spherical GNPs. The DOX influence after conjugation with PVP-GNPs was measured at ∼490 nm. As shown in Figure 4B, the UV−vis results exhibited two signals with precisely tuned positions of a weak transverse plasmon band at ∼523 nm and, most importantly, a longitudinal

plasmon intense band range ranges from ∼740 to ∼780 nm, indicating the effective surface modification of PVP-GNPs with DOX molecules.[10] The change in the red shift from ∼740 to ∼780 nm depicts the successful conjugation of DOX molecules with PVP-GNPs. Moreover, after the surface decoration of PVP-GNPs with DOX, strong broadband with an important red shift in SPR indicates that DOX stabilized the PVP-GNP solution. In addition, the strong absorption band of PVP-GNPs after conjugation with DOX could be associated with the change in the refractive index of PVP-GNPs. The spectral data of PVP-GNPs-DOX with an important red shift in the SPR position also indicate their excellent colloidal stability in aqueous solution.

2.4. FTIR Analysis. The FTIR spectral analysis was performed to study the possible reaction mechanism and the existence of various functional groups among PVP, DOX, and PVP-GNPs-DOX. For this reason, all of the samples were first freeze-dried, and solid samples were then ground and mixed with potassium bromide (KBr), which generally does not absorb mid-infrared wavelength light in the range of 4000−500 cm^{-1}. The resulting mixture was then analyzed after pressing into a pellet in an evacuated chamber. Figure 5 shows the
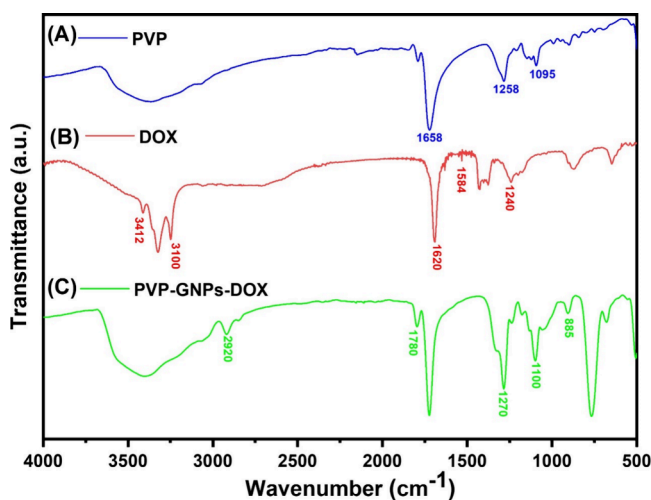

Figure 5. FTIR spectra of PVP (A), DOX (B), and PVP-GNPs-DOX (C).

FTIR spectra of pure PVP, DOX, and PVP-GNPs-DOX. The FTIR spectra of pure PVP (Figure 5A) reveal the characteristic signals at around 1658 and ∼1258 cm^{-1}, representing the C=O (carbonyl/carboxyl) groups and N−H stretching vibrations, respectively.[36] The broad absorption band observed at around 3450−3350 cm^{-1} corresponded to the hydroxyl group. Subsequently, PVP spectra also suggest the more obvious moisture uptake by C=O groups. In the case of pure DOX, the prominent peaks appeared at around 3412, 3100, 1620, 1584, and 1240 cm^{-1}, confirming the presence of O−H and N−H stretching vibrations, N−H bending of the primary amine group, and the C−O−C asymmetric stretching vibration, respectively.[37] Consequently, the hydroxyl and amino groups of DOX play an important role in the coordination of carboxyl and carbonyl groups to form hydrazone and an amido link. Additionally, both hydrazone linkages and amidation are pH-sensitive and capable of releasing the therapeutic drug at the acidic pH of the tumor or infection sites due to their faster hydrolysis rate at acidic

pH.[36,37] All of the major principal characteristic peaks of PVP and DOX appeared in PVP-GNPs-DOX spectra with slight shifts, confirming the existence of hydroxyl, carboxyl, and carbonyl groups on the outer surface of the GNPs. In addition, these functional groups can form chemical bonds with other functional groups of PVP and DOX. Moreover, because of a low amount of DOX in PVP-GNPs-DOX, the significant absorption bands of DOX were completely overlapped with PVP absorption bands, which further confirms the successful loading of DOX onto PVP-GNPs.

2.5. TEM Analysis. Analytical TEM, as an effective high-resolution imaging technique with the ability to visualize the atomic structures and morphology, was employed to analyze the size and crystallographic structure of as-synthesized PVP-GNPs and PVP-GNPs-DOX. TEM images indicate that all of the GNPs in PVP-GNPs and PVP-GNPs-DOX were highly crystalline, exhibited a spherical shape, and were uniformly distributed without accumulation or aggregation (Figure 6). Digital image processing methods such as ImageJ (Java-based, public domain), which is generally a very convenient and cost-effective approach to measuring the different physical properties such as texture and color composition, in particular the particle size, were used for accurate analysis of the particle size distribution. In order to represent the particle size distribution, a histogram or frequency diagram was constructed by randomly selecting at least 50 particles.

The TEM images and particle size distribution histogram (Figure 6A−D) elucidate that GNPs in PVP-GNPs and PVP-GNPs-DOX had average particle diameters of 10.73 ± 1.55 and 26.35 ± 2.13 nm, respectively. Additionally, the TEM image of PVP-GNPs-DOX nanoconjugates indicates a slight accumulation and irregularity in the GNP shape (Figure 6C), thereby increasing the particle size. Typically, DOX-conjugated PVP-GNPs have a greater particle size distribution (Figure 6D), which could be associated with the surface modification artifacts and drug loading, whereas organic materials suspended in GNP solution significantly decrease the electrostatic repulsions among head-to-head GNPs, thus favoring colloidal agglomeration.[38] This difference between the size of GNPs recorded by TEM and DSL could be due to the different operations of TEM and DLS techniques, though the extent and nature of these effects differ for each technique. TEM offers high spatial resolution down to the atomic scale and allows for direct imaging of nanomaterials without relying on indirect inference methods, making it more accurate for shape and size distribution determination than DLS. It is evident from the HR-TEM image (Figure 6E) that a single nanocrystal with clear lattice fringes has a spacing of 0.23 nm, preferentially showing that the growth of GNPs occurred along the (111) plane, validating the XRD results and again confirming the face-centered cubic structure of GNPs. Moreover, the lattice fringes and SAED pattern (Figure 6F) with sharp bright spots from single crystal ring patterns corresponding to the (111), (200), (220), and (311) planes confirm the highly crystalline nature of GNPs.

The GNPs with tunable surfaces have been widely used in therapeutic delivery and tumor targeting.[9] However, stability and aggregation influence the GNPs' fate in aqueous environments subject to the organic matter compositions, ionic strength, and pH. The stabilizing agents and biochemical reactions' pH may affect the surface charge stability of GNPs and, in turn, particle dispersion and behavior for specific exposure to organisms.[9,38] A low pH (<5) tends to increase
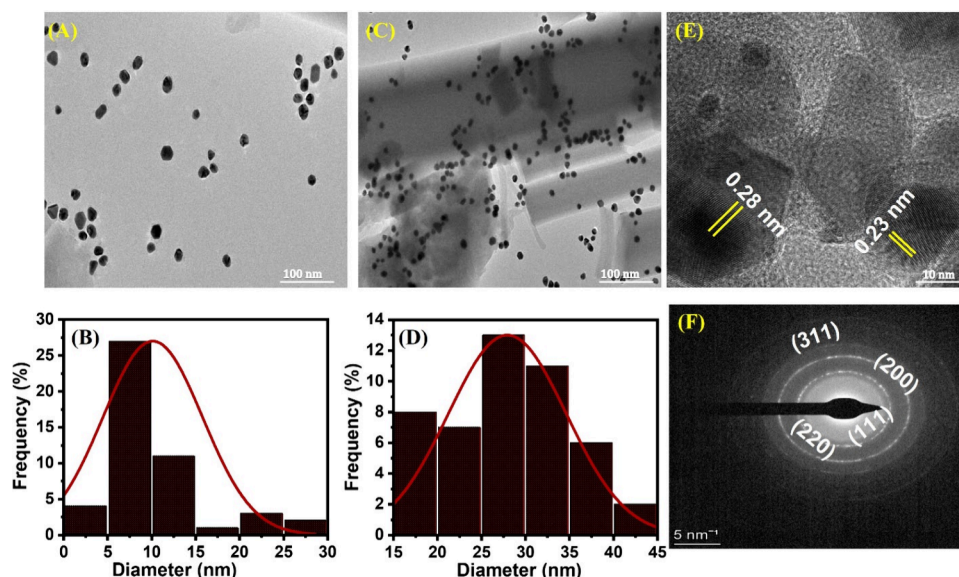
Figure 6. TEM image (A) and corresponding size distribution histogram of PVP-GNPs (B). TEM image (C) and size distribution histogram of PVP-GNPs-DOX (D), HR-TEM image (E), and SAED of PVP-GNPs-DOX (F).
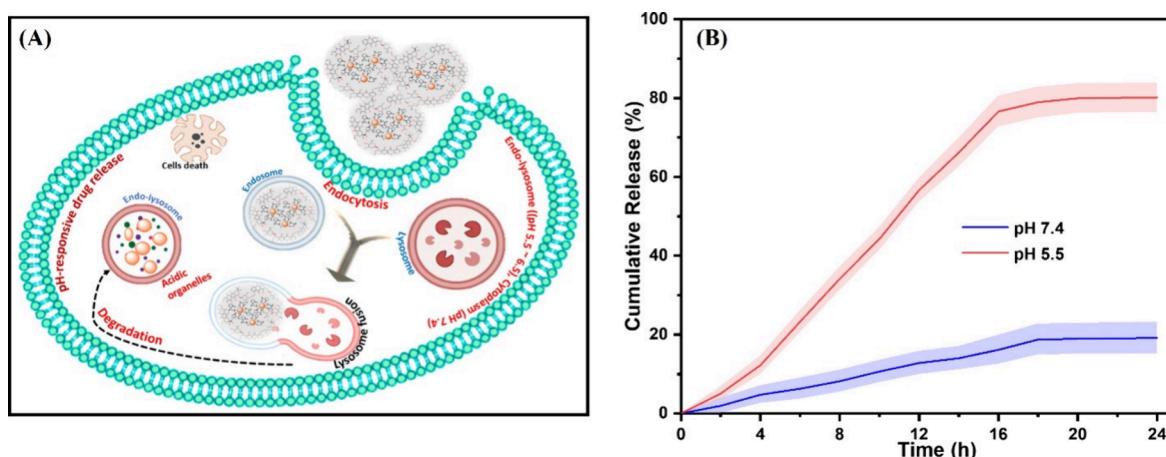

Figure 7. Schematic illustration of DOX conjugation and release in the acidic compartment due to the acid-catalyzed hydrolysis of the hydrazone linker (A) and in vitro DOX release kinetics from PVP-GNPs-DOX (B). Data was presented as the mean ± SD of three independent experiments.

oxidation instead of reduction, and a high pH (≥9) favors a shortened precipitation time and increasing reduction rate, which also means increasing the GNPs size. Thus, if desired, the particle agglomeration and aggregation processes were controlled to some extent by controlling the pH of the reaction mixture.[15] From the precipitation profile, pH 7−8 of the working solution is highly desirable for synthesizing smaller nanoparticles. Moreover, the chemistry of the colloid is key to stability along with the presence of polyvalent ions, pH, and concentration. PVP, a linear polyelectrolyte polymer, is characterized by its high affinity and forms complexes with various compounds due to the presence of a strong polar group (vinyl ring). In the presence of PVP molecules, the gold cations (Au^{3+}) were reduced to gold atoms[33] that further agglomerate to small GNP clusters, and as a result, PVP-GNPs-DOX was poorly protected against agglomeration. Overall, these results indicate good monodispersity and stability of PVP-GNPs-DOX with slight particle aggregation.

2.6. Drug Release Kinetics. Initially, the GNP surfaces were tuned with PVP, a pH-sensitive polymer and hydrazine-terminated linker (EDC/NHS) through π−π interactions, and

then EDC/NHS-capped PVP-GNPs were conjugated with DOX through its ketone and EDC/NHS coupling conjugation method, yielding a pH-responsive PVP-GNPs-DOX nano-formulation (Figure 7A). The pH-responsive in vitro release kinetics of the PVP-GNPs-DOX nanoformulation were investigated under different pH values (7.4 and 5.5). These two pH values were chosen according to their physiological relevance to the pH of intra- and extracellular tumor cells.[39] Figure 7B illustrates the DOX release kinetics of PVP-GNPs-DOX at two pH values (7.4, and 5.5) of buffer solutions. Over 24 h, PVP-GNPs-DOX was able to retain a significant fraction of DOX at pH 7.4. In addition, only approximately 19% of DOX was released sustainably, preferentially suggesting that an amide linkage between PVP-GNPs and DOX is quite stable at pH 7.4, with a low level of systemic toxicity. However, upon exposure to acidic subcellular compartments, the hydrazine linker installed on PVP-GNPs surfaces could facilitate the cleavage of drug molecules by the chemo-selective nature of the linker. For an effective drug delivery system, the DOX molecules have to leave the cross-linker and inhibit the formation of stable cation−π interactions during the physical

encapsulation.[14] Therefore, to confirm this hypothesis, we changed the pH of the release medium to pH 5.5. At high pH values, since most of the DOX was retained inside the PVP-GNPs in the first 24 h when the bond between the cross-links and DOX was cleaved under acidic conditions, there was no evidence of burst release of DOX. Unlike the DOX release rate at pH 7.4, a significantly accelerated release rate of DOX was observed under the latter condition, possibly due to the pH-responsive behavior of PVP and deformation of the bond between the PVP-GNPs and DOX in an acidic environment. Within 24 h, it was found that DOX release kinetics from PVP-GNPs-DOX were much higher at acidic pH than at neutral pH (Figure 7B). Subsequently, approximately 80% of the DOX release was detected at pH 5.5, suggesting the capability of the PVP-GNPs-DOX to be efficiently utilized for on-demand controlled drug release at a desired site, ultimately resulting in improved toxic effects against ovarian cancer.

2.7. Cell Viability Assay. Biocompatibility and potential cytotoxicity of the PVP-GNPs and PVP-GNPs-DOX are necessary for their successful regulatory approval in the biomedical field. Therefore, we adopted the in vitro cell culture technique to interrogate the potential mechanistic aspect of cytotoxicity induced by PVP-GNPs and PVP-GNPs-DOX. The cytotoxicity results induced by PVP-GNPs, PVP-GNPs-DOX, and DOX against the HeLa cell line are presented in Figure 8. The microscopic images of HeLa cells treated with
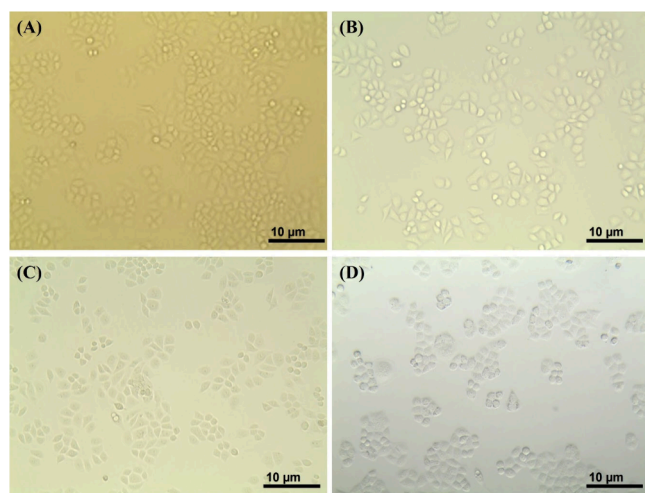

Figure 8. Morphological changes in the HeLa cells control (A). Cells incubated with the same concentration (200 μg/mL) of PVP-GNPs (B), PVP-GNPs-DOX (C), and DOX (D).

PVP-GNPs (Figure 8B), PVP-GNPs-DOX (Figure 8C), and DOX (Figure 8D) were compared with untreated control cells (Figure 8A). Notably, it was observed that HeLa cells treated with PVP-GNPs (Figure 7B) had morphology similar to those obtained from untreated control cells (Figure 7A) and did not produce acute cytotoxicity.

On the other hand, various morphological changes were seen in HeLa cells when treated with PVP-GNPs-DOX (Figure 8C) and DOX (Figure 8D). The PVP-GNPs-DOX induces cell communication inhabitation, cell clumping, shape alterations, and cell death, where the control or cells treated with PVP-GNPs were active. Moreover, these results support the indication that HeLa cells were strongly attached to the PVP-GNPs, PVP-GNPs-DOX, and DOX. PVP-GNPs, PVP-GNPs-DOX, and DOX significantly initiated the apoptosis

pathways by reactive oxygen species, thereby leading to alterations in cell morphology and cell death.

To examine the cytotoxicity induced by PVP-GNPs, PVP-GNPs-DOX, and DOX alone, HeLa cells were incubated with an increasing concentration of either PVP-GNPs, PVP-GNPs-DOX, or DOX only. The cell viability was investigated by MTT assay, and the results were presented as a percentage (100%) of the control cells. The MTT-assay analysis elucidates the levels of inhibitory effects observed as a function of increasing concentration of PVP-GNPs, PVP-GNPs-DOX, and DOX with respect to the proliferation of HeLa cells. As shown in Figure 9A, at all of the tested concentrations, the PVP-GNPs did not contribute to the overall toxicity, strongly suggesting that PVP-GNPs alone can be attributed to having excellent biocompatible. However, HeLa cells treated with increasing concentrations of PVP-GNPs-DOX or DOX alone showed dose-dependent cytotoxicity for the population of viable cells as compared to that of PVP-GNPs. As shown in Figure 9A, it was found that the cell viability index of PVP-GNPs-DOX for all of the tested concentrations was significantly comparable to that of free DOX. These results further support the dissociation and sustainable DOX release from PVP-GNPs-DOX, which is then quickly transported into the cells and enters the nuclei of the cells for selective targeting,[10,15] leading to a significantly higher surge in the toxic effect. Approximately 78.35 and 74.95% of HeLa cells were dead after being incubated for 24 h with 200 μg/mL PVP-GNPs-DOX and free DOX, respectively. In addition, no significant cancer cell inhibition was observed by increasing the concentration of PVP-GNPs.

Next, the correlation between the test concentrations of PVP-GNPs (control), PVP-GNPs-DOX, and DOX and cell viability (%) after 24 h of exposure to HeLa cells was analyzed for the half maximal inhibitory concentration (IC$_{50}$) (Figure 9B). IC$_{50}$ refers to the most commonly used parameter that is required for 50% inhibition of cell proliferation. Moreover, IC$_{50}$ analysis facilitates the on-target activity in lead optimization and guides the large-scale development of useful methods for drug discovery with more potency. Figure 9B shows the dose−response curves and IC$_{50}$ values (inset) of the control, PVP-GNPs-DOX, and DOX from the MTT assay. The control group exhibits an IC$_{50}$ value of above 295 μM. This indicates that, within the measured concentration range, PVP-GNPs were significantly less toxic to HeLa cells. However, there was a considerable drop in the IC$_{50}$ values of PVP-GNPs-DOX (14.6 μM) when compared to the IC$_{50}$ values of free DOX (24.8 μM). Lower IC$_{50}$ values of PVP-GNPs-DOX exhibited their significant potent effect against HeLa cells, having potency very close to that of corresponding free DOX.

Some conflicting controversy about the size-dependent cytotoxicity of GNPs exists; however, it is still an unknown parameter as to whether the size or surface treatment (coating or noncoating) of GNPs induces cellular damage or concerns cytotoxicity.[40] In this regard, it has been reported that smaller GNPs (<30 nm size) showed higher cytotoxicity than larger GNPs (≥50 nm).[41] In contrast, the safety and toxicological potential of GNPs depend not only on the size but also on the shape, microstructures, and surface coating.[42] Taken together, these results suggest that neither the surface modification characteristics nor the size of GNPs could exert severe cytotoxicity but the shape and intracellular modifications of GNPs could be responsible for causing toxicity. These
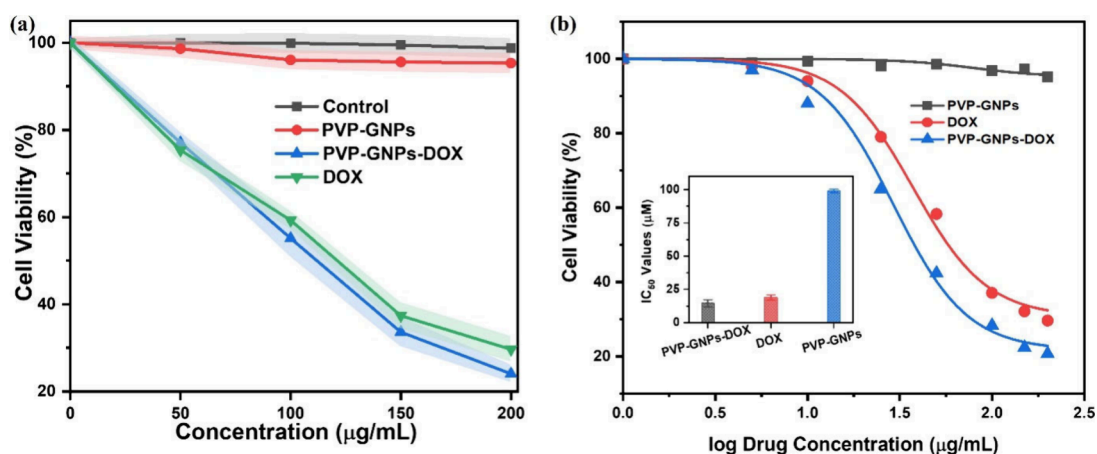
Figure 9. In vitro cytotoxicity profile determined by MTT assay for 24 h exposure under the various concentrations of PVP-GNPs, PVP-GNPs-DOX, and DOX (a). The cell viability of the control or untreated cells was set to 100%. The dose−response curve and calculation of IC50 values (inset, bar graph) at which the curve passes through the 50% inhibition level for the control group, PVP-GNPs-DOX, and DOX (b).

characteristics of GNPs in turn could be controlled during synthesis and under the processing conditions.

In addition, our results indicate that higher therapeutic efficiency was achieved through the concurrent release of DOX from PVP-GNPs-DOX in the acidic environment of the tumor. Furthermore, this study proves the ability of PVP-GNPs-DOX nanoconjugates to suppress the survival rates of HeLa cells, which makes them more sensitive to bypassing MDR and decreasing the negative effects of medications. Moreover, the high surface-to-volume ratio of PVP-GNPs is an excellent opportunity for enhancing the loading efficiency of chemotherapeutic agents, thereby achieving higher tumor extravasation. The PVP layer not only acts as a stabilizer but also enhances the circulation time and helps to protect the GNPs from rapid reticuloendothelial clearance.

3. CONCLUSIONS

In order to determine the precise trajectory of the new class of tunable PVP-GNPs as possible drug delivery agents, we effectively decorated their surfaces with the model anticancer drug DOX using a simple, cost-effective aqua route. The morphology and electronic properties of the as-synthesized PVP-GNPs and PVP-GNPs-DOX nanoconjugates were systematically characterized and investigated by different microscopic and spectroscopic techniques for their potential medical applications as cargo vehicles that ideally promote the suppression of cancer cell growth. In vitro cytotoxicity analysis and concentration-dependent targeting capabilities of PVP-GNPs-DOX were evaluated in the HeLa cell model. The designed PVP-GNPs-DOX primarily possesses dose-dependent potent cell death activities. These findings further validate the uptake kinetics and/or cellular target specificities of PVP-GNPs-DOX and could be potentially used as a synergistic therapeutic delivery platform for various biomedical applications such as anticancer activities. In light of these results, we believe that by improving the biodistribution and bioavailability profiles, this study offers a great opportunity to design a next-generation delivery system and opens new horizons for the active targeting of ovarian cancers, with the hope of covering the existing gap in clinical settings.

4. MATERIALS AND METHODS

4.1. Chemicals. Gold(III) chloride tetra-hydrate (HAuCl$_4$·4H$_2$O, 99%), sodium citrate, and sodium hydroxide (NaOH, 97%) were purchased from Sinopharm (China). N-Hydroxy succinimide (NHS), polyvinylpyrrolidones (PVP-40), 1-ethyl-3-(3-dimethyl aminopropyl) carbodiimide (EDC), and DOX-hydrochloride (98%) were purchased from Merck (China). Deionized water (DI) (Shanghai Hitech-Instruments Apparatus) was used throughout the experiments to prepare all of the stock solutions. Dulbecco's modified Eagle's medium (DMEM), dimethyl sulfoxide (DMSO), fetal bovine serum (FBS), phosphate-buffered saline (PBS), minimum essential medium (MEM), dimethyl-thiazolyl tetrazolium bromide (MTT) and other chemicals were obtained from Aladdin (China) and used as provided.

4.2. Synthesis of PVP-Stabilized GNPs. Unless otherwise stated, the following standard conditions applied. All glassware was washed with freshly prepared aqua regia followed by two rinses with DI water and drying in an oven. All of the analytical-grade reagents that have been used during the experiment were purchased from commercial vendors. The PVP-stabilized GNPs were synthesized following previously reported protocols[27,38] with slight modification, which involves the reduction of Au (III) to Au^0 from chloroauric acid by sodium citrate. Briefly, 100 mL of an aqua solution of chloroauric acid (1.0 mM) was boiled under stirring in a three-necked round-bottomed flask. Subsequently, 2 mL of a 1% sodium citrate freshly prepared solution was added under reflux, and the reaction flask was removed from the heat when the solution turned burgundy red and was kept in an ice bath for 15 min. Furthermore, PVP was conjugated to the surfaces of citrate-capped GNPs, as previously described.[38] In detail, first 1 g of PVP was dispersed ultrasonically in 5 mL of water, followed by mixing with a citrate-capped GNP solution and then stirring at 25 °C overnight. The excess PVP was separated by centrifugation (10,000 rpm, 15 min) and two washings with DI water. The supernatant was aspirated, and obtained PVP-GNPs were resuspended in DI water for further modification and use.

4.3. Synthesis of DOX-Loaded PVP-GNPs. To synthesize DOX-loaded PVP-GNPs, initially 1 mL of EDC and NHS (1:1, 10.8 mg/mL) was dissolved in a 50 mL solution of PVP-GNPs. The suspension was then stirred for 30 min at room

temperature. Subsequently, 4.5 mg of DOX was dissolved in 5 mL of DMSO ultrasonically and then mixed with a PVP-GNPs, EDC/NHS suspension. The suspension was then placed in the dark for 24 h, followed by stirring at room temperature. Later, when the set time was reached, the unbound DOX was removed by centrifugation (10,000 rpm, for 5 min) and washed twice with pH 7.4 PBS. The supernatant was aspirated, and the PVP-GNPs-DOX pellet was dispersed in PBS for further characterization.

4.4. Characterization. The physicochemical properties of PVP-GNPs and PVP-GNPs-DOX were determined with a Rigaku D Max-2550VB/PC X-ray diffraction (XRD) instrument, and a scanning transmission electron microscopy (S/TEM) and selected area electron diffraction (SAED) study was performed with a Tecnai G2 F20 S-Twin TEM. Fourier transform infrared (FTIR) spectroscopy was carried out with an FT/IR-6300 instrument (Jasco) at $400-4000$ cm^{-1}, and ultraviolet–visible (UV–vis) absorption analysis was performed with a Lambda 850 (PerkinElmer) instrument. The hydrodynamic particle size and zeta potential measurements were performed with dynamic light scattering (DLS) and microelectrophoresis (ME) at room temperature using a Zetasizer Nano ZS90 (Malvern).

4.5. In Vitro Release Kinetics. In vitro release kinetics of DOX from PVP-GNPs-DOX were determined at 37 °C in buffers (PBS pH 7.4, acetate pH 5.2) under sink conditions. During the release experiment, the temperature was kept constant by a water bath. The PVP-GNPs-DOX solution was protected from light with aluminum foil. Typically, 1 mL of a PVP-GNPs-DOX solution was dialyzed against 10 mL of release buffer saline to form a homogeneous suspension and placed in dialysis tubes (CelluSep, T-Series, molecular weight cutoff 6–8 kDa, Shanghai Science Biotechnology), and the tubes were then magnetically stirred (200 rpm) and maintained at 37 °C. At predetermined time intervals, the outer solution was taken out and exchanged with the same amount of fresh buffer solution. The amount of DOX was quantitatively measured by analyzing the DOX UV absorbance at $\lambda = 495$ nm. For each sample, the release experiments were performed in triplicate, and the error bars in the plot represent the standard deviation.

4.6. In Vitro Cytotoxicity Studies. The HeLa cell line was used to investigate the in vitro toxicity of PVP-GNPs and PVP-GNPs-DOX. The cell culture experiment was performed under a sterile type-II laminar flow hood, as previously described.[14] Before the experiment, the entire apparatus was sterilized in an autoclave. An incubator and hemocytometer were used to maintain the temperature and determination of cell confluence, respectively. The DMEM along with 10% FBS, sodium bicarbonate (1.5 g/L), and penicillin-streptomycin (100 mg/mL) was used for cell culturing. The cells were cultivated in a 96-well microplate and maintained at 37 °C for 24 h to grow in confluence (80–90%) under moist conditions with 5% CO_2 and 95% air. After the incubation, the morphological changes in the cells were observed under an inverted biological microscope (AE31 series, Motic Instruments, Germany). The MTT assay was used to investigate the complement-mediated toxicity of PVP-GNPs, PVP-GNPs-DOX, and DOX alone. Before the addition of MTT, all of the tested samples were prepared by transferring them into water (1 mg/mL). For comparison, DOX alone with five growing concentrations of 0, 50, 100, 150, and 200 μg/mL was also used and added in triplicate to each well of confluent cells.

After that, the treated cells were incubated overnight at 37 °C and then rinsed with PBS. In each well of the plate, 20 μL of MTT solution was added and the cells were again incubated for 3 h. The quantity of formazan was analyzed by recording the plate absorbance at 570 nm using a Victor3 spectrophotometer (PerkinElmer), and data were presented here as the mean ± standard deviation. The optical density or absorbance values were converted to (%) cell viability by using the simple equation

$$(\%) \text{ cell viability} = [S/C] \times 100$$

where S and C represent the absorbance of sample and control wells, respectively.

■ AUTHOR INFORMATION

Corresponding Authors

Muhammad Umar Farooq − *School of Chemistry and Chemical Engineering, Shanghai Jiao Tong University, 200240 Shanghai, China; A. M. Butlerov Institute of Chemistry, Kazan Federal University, Kazan 420008, Russian Federation;* ⓘ orcid.org/0000-0001-8804-9754; Email: umar@sjtu.edu.cn

Anipa Tapalova − *Department of Biology, Geography and Chemistry, Korkyt Ata Kyzylorda University, Kyzylorda 120014, Kazakhstan;* Email: anipa52@mail.ru

Mohamed M. Makhlouf − *Department of Sciences and Technology, Ranyah University College, Taif University, Taif 21944, Saudi Arabia;* ⓘ orcid.org/0000-0002-7413-4322; Email: m.makhlouf@tu.edu.sa

Authors

Alexey P. Dovzhenko − *Arbuzov Institute of Organic and Physical Chemistry, FRC Kazan Scientific Center of RAS, Kazan 420088, Russian Federation*

Rustem R. Zairov − *A. M. Butlerov Institute of Chemistry, Kazan Federal University, Kazan 420008, Russian Federation; Arbuzov Institute of Organic and Physical Chemistry, FRC Kazan Scientific Center of RAS, Kazan 420088, Russian Federation;* ⓘ orcid.org/0000-0002-1699-6741

Gulmira Abyzbekova − *Department of Biology, Geography and Chemistry, Korkyt Ata Kyzylorda University, Kyzylorda 120014, Kazakhstan*

Moussab Harb − *Department of Physics, Faculty of Science, King Abdulaziz University, Jeddah 21589, Saudi Arabia*

Bassim Arkook − *Department of Physics, Faculty of Science, King Abdulaziz University, Jeddah 21589, Saudi Arabia;* ⓘ orcid.org/0000-0002-4968-0954

Nurgali Akylbekov − *Laboratory of Engineering Profile "Physical and Chemical Methods of Analysis", Korkyt Ata Kyzylorda University, Kyzylorda 120014, Kazakhstan;* ⓘ orcid.org/0000-0002-7584-9741

Complete contact information is available at:
https://pubs.acs.org/10.1021/acsomega.4c04134

Notes

The authors declare no competing financial interest.

REFERENCES

(1) Melaku, Y. A.; Appleton, S. L.; Gill, T. K.; Ogbo, F. A.; Buckley, E.; Shi, Z.; Driscoll, T.; Adams, R.; Cowie, B. C.; Fitzmaurice, C. Incidence, prevalence, mortality, disability-adjusted life years and risk factors of cancer in Australia and comparison with OECD countries, 1990−2015: findings from the Global Burden of Disease Study 2015. *Cancer epidemiology* **2018**, *52*, 43−54.

(2) Hoeijmakers, J. H. DNA damage, aging, and cancer. *New England journal of medicine* **2009**, *361* (15), 1475−1485.

(3) Duenas-Gonzalez, A.; Campbell, S. Global strategies for the treatment of early-stage and advanced cervical cancer. *Current opinion in obstetrics & gynecology* **2016**, *28* (1), 11−17.

(4) Hawley, S. T.; Lantz, P. M.; Janz, N. K.; Salem, B.; Morrow, M.; Schwartz, K.; Liu, L.; Katz, S. J. Factors associated with patient involvement in surgical treatment decision making for breast cancer. *Patient education and counseling* **2007**, *65* (3), 387−395.

(5) Han, Q.; Fang, Z.; Lin, R.; Chen, J.; Wei, X.; Gong, C.; Yang, Z.; Zou, P.; Zhu, J.; Xing, L.; et al. Piezo-photodynamic therapy of Au@PEG-ZnO nanostructures enabled with a battery-free wireless cancer therapeutic dot. *Nano Energy* **2024**, *125*, 109530.

(6) Yang, C. J.; Chithrani, D. B. Nuclear Targeting of Gold Nanoparticles for Improved Therapeutics. *Current topics in medicinal chemistry* **2016**, *16* (3), 271−280.

(7) Yang, M.; Li, J.; Gu, P.; Fan, X. The application of nanoparticles in cancer immunotherapy: Targeting tumor microenvironment. *Bioactive materials* **2021**, *6* (7), 1973−1987.

(8) Singh, A. P.; Biswas, A.; Shukla, A.; Maiti, P. Targeted therapy in chronic diseases using nanomaterial-based drug delivery vehicles. *Signal transduction and targeted therapy* **2019**, *4*, 33.

(9) Farooq, M. U.; Sahin, Y. M.; Naz, M. Y.; Ijaz, S.; Shukrullah, S.; Makhlouf, M. M. Surface engineered AuNPs for paclitaxel-loaded bleomycin delivery as a supplementation therapy. *Applied Nanoscience* **2022**, *12*, 3883.

(10) Aryal, S.; Grailer, J. J.; Pilla, S.; Steeber, D. A.; Gong, S. Doxorubicin conjugated gold nanoparticles as water-soluble and pH-responsive anticancer drug nanocarriers. *J. Mater. Chem.* **2009**, *19* (42), 7879.

(11) Wang, W.; Wang, J.; Ding, Y. Gold nanoparticle-conjugated nanomedicine: design, construction, and structure-efficacy relationship studies. *Journal of materials chemistry. B* **2020**, *8* (22), 4813−4830.

(12) Nilubol, N.; Yuan, Z.; Paciotti, G. F.; Tamarkin, L.; Sanchez, C.; Gaskins, K.; Freedman, E. M.; Cao, S.; Zhao, J.; Kingston, D. G. I.; et al. Novel Dual-Action Targeted Nanomedicine in Mice With Metastatic Thyroid Cancer and Pancreatic Neuroendocrine Tumors. *Journal of the National Cancer Institute* **2018**, *110* (9), 1019−1029.

(13) Lin, G.; Mi, P.; Chu, C.; Zhang, J.; Liu, G. Inorganic Nanocarriers Overcoming Multidrug Resistance for Cancer Theranostics. *Advanced Science* **2016**, *3* (11), 1600134.

(14) Farooq, M. U.; Naz, M. Y.; Hussain, M. I.; Shukrullah, S.; Makhlouf, M. M. Smart Therapeutic Strategy of pH-Responsive Gold Nanoparticles for Combating Multidrug Resistance. *Particle & Particle Systems Characterization* **2021**, *38* (7), 2100073.

(15) Khandelia, R.; Jaiswal, A.; Ghosh, S. S.; Chattopadhyay, A. Gold nanoparticle-protein agglomerates as versatile nanocarriers for drug delivery. *Small* **2013**, *9* (20), 3494−3505.

(16) Lee, C. S.; Kim, T. W.; Oh, D. E.; Bae, S. O.; Ryu, J.; Kong, H.; Jeon, H.; Seo, H. K.; Jeon, S.; Kim, T. H. In Vivo and In Vitro Anticancer Activity of Doxorubicin-loaded DNA-AuNP Nanocarrier for the Ovarian Cancer Treatment. *Cancers* **2020**, *12* (3), 634.

(17) Petryayeva, E.; Krull, U. J. Localized surface plasmon resonance: Nanostructures, bioassays and biosensing—A review. *Anal. Chim. Acta* **2011**, *706* (1), 8−24.

(18) Vines, J. B.; Yoon, J. H.; Ryu, N. E.; Lim, D. J.; Park, H. Gold Nanoparticles for Photothermal Cancer Therapy. *Frontiers in chemistry* **2019**, *7*, 167.

(19) Manivasagan, P.; Bharathiraja, S.; Bui, N. Q.; Lim, I. G.; Oh, J. Paclitaxel-loaded chitosan oligosaccharide-stabilized gold nanoparticles as novel agents for drug delivery and photoacoustic imaging of cancer cells. *International journal of pharmaceutics* **2016**, *511* (1), 367−379.

(20) Boisselier, E.; Astruc, D. Gold nanoparticles in nanomedicine: preparations, imaging, diagnostics, therapies and toxicity. *Chem. Soc. Rev.* **2009**, *38* (6), 1759−1782.

(21) Wilhelm, S.; Tavares, A. J.; Dai, Q.; Ohta, S.; Audet, J.; Dvorak, H. F.; Chan, W. C. W. Analysis of nanoparticle delivery to tumours. *Nature Reviews Materials* **2016**, *1* (5), 16014.

(22) Du, Y.; Xia, L.; Jo, A.; Davis, R. M.; Bissel, P.; Ehrich, M. F.; Kingston, D. G. I. Synthesis and Evaluation of Doxorubicin-Loaded Gold Nanoparticles for Tumor-Targeted Drug Delivery. *Bioconjugate Chem.* **2018**, *29* (2), 420−430.

(23) Carvalho, F. S.; Burgeiro, A.; Garcia, R.; Moreno, A. J.; Carvalho, R. A.; Oliveira, P. J. Doxorubicin-induced cardiotoxicity: from bioenergetic failure and cell death to cardiomyopathy. *Medicinal research reviews* **2014**, *34* (1), 106−135.

(24) Wang, F.; Wang, Y. C.; Dou, S.; Xiong, M. H.; Sun, T. M.; Wang, J. Doxorubicin-tethered responsive gold nanoparticles facilitate intracellular drug delivery for overcoming multidrug resistance in cancer cells. *ACS Nano* **2011**, *5* (5), 3679−3692.

(25) Chaudhary, A.; Dwivedi, C.; Gupta, A.; Nandi, C. K. One pot synthesis of doxorubicin loaded gold nanoparticles for sustained drug release. *RSC Adv.* **2015**, *5* (118), 97330−97334.

(26) Mirza, A. Z.; Shamshad, H. Fabrication and characterization of doxorubicin functionalized PSS coated gold nanorod. *Arabian Journal of Chemistry* **2019**, *12* (1), 146−150.

(27) Alijagic, A.; Bonura, A.; Barbero, F.; Puntes, V. F.; Gervasi, F.; Pinsino, A. Immunomodulatory Function of Polyvinylpyrrolidone (PVP)-Functionalized Gold Nanoparticles in Vibrio-Stimulated Sea Urchin Immune Cells. *Nanomaterials* **2021**, *11* (10), 2646.

(28) Franco, P.; De Marco, I. The Use of Poly(N-vinyl pyrrolidone) in the Delivery of Drugs: A Review. *Polymers (Basel)* **2020**, *12* (5), 1114.

(29) Khandekar, S. V.; Kulkarni, M. G.; Devarajan, P. V. Polyaspartic acid functionalized gold nanoparticles for tumor targeted doxorubicin delivery. *J. Biomed Nanotechnol* **2014**, *10* (1), 143−153.

(30) Philip, D. Biosynthesis of Au, Ag and Au-Ag nanoparticles using edible mushroom extract. *Spectrochimica Acta Part A: Molecular and Biomolecular Spectroscopy* **2009**, *73* (2), 374−381.

(31) Wang, W.; Ding, X.; Xu, Q.; Wang, J.; Wang, L.; Lou, X. Zeta-potential data reliability of gold nanoparticle biomolecular conjugates and its application in sensitive quantification of surface absorbed protein. *Colloids Surf. B Biointerfaces* **2016**, *148*, 541−548.

(32) Martínez, J. C.; Chequer, N. A.; González, J. L.; Cordova, T. Alternative Metodology for Gold Nanoparticles Diameter Characterization Using PCA Technique and UV-VIS Spectrophotometry. *Nanoscience and Nanotechnology* **2012**, *2* (6), 184−189.

(33) Li, C.; Fan, F.; Yin, B.; Chen, L.; Ganguly, T.; Tian, Z. Au+-cetyltrimethylammonium bromide solution: A novel precursor for seed-mediated growth of gold nanoparticles in aqueous solution. *Nano Research* **2013**, *6* (1), 29−37.

(34) Link, S.; El-Sayed, M. A. Optical properties and ultrafast dynamics of metallic nanocrystals. *Annu. Rev. Phys. Chem.* **2003**, *54*, 331−366.

(35) Kamalakannan, R.; Mani, G.; Muthusamy, P.; Susaimanickam, A. A.; Kim, K. Caffeine-loaded gold nanoparticles conjugated with PLA-PEG-PLA copolymer for in vitro cytotoxicity and anti-inflammatory activity. *Journal of Industrial and Engineering Chemistry* **2017**, *51*, 113−121.

(36) Dhumale, V. A.; Gangwar, R. K.; Datar, S. S.; Sharma, R. B. Reversible Aggregation Control of Polyvinylpyrrolidone Capped Gold Nanoparticles as a Function of pH. *Materials Express* **2012**, *2* (4), 311−318.

(37) Alizadeh, N.; Akbari, V.; Nurani, M.; Taheri, A. Preparation of an injectable doxorubicin surface modified cellulose nanofiber gel and evaluation of its anti-tumor and anti-metastasis activity in melanoma. *Biotechnology progress* **2018**, *34* (2), 537−545.

(38) Alijagic, A.; Barbero, F.; Gaglio, D.; Napodano, E.; Benada, O.; Kofronova, O.; Puntes, V. F.; Bastus, N. G.; Pinsino, A. Gold nanoparticles coated with polyvinylpyrrolidone and sea urchin extracellular molecules induce transient immune activation. *Journal of hazardous materials* **2021**, *402*, 123793.

(39) Danhier, F.; Feron, O.; Préat, V. To exploit the tumor microenvironment: Passive and active tumor targeting of nanocarriers for anti-cancer drug delivery. *J. Controlled Release* **2010**, *148* (2), 135−146.

(40) Sani, A.; Cao, C.; Cui, D. Toxicity of gold nanoparticles (AuNPs): A review. *Biochemistry and biophysics reports* **2021**, *26*, 100991.

(41) Pan, Y.; Neuss, S.; Leifert, A.; Fischler, M.; Wen, F.; Simon, U.; Schmid, G.; Brandau, W.; Jahnen-Dechent, W. Size-dependent cytotoxicity of gold nanoparticles. *Small* **2007**, *3* (11), 1941−1949.

(42) Niidome, T.; Yamagata, M.; Okamoto, Y.; Akiyama, Y.; Takahashi, H.; Kawano, T.; Katayama, Y.; Niidome, Y. PEG-modified gold nanorods with a stealth character for in vivo applications. *Journal of controlled release: official journal of the Controlled Release Society* **2006**, *114* (3), 343−347.